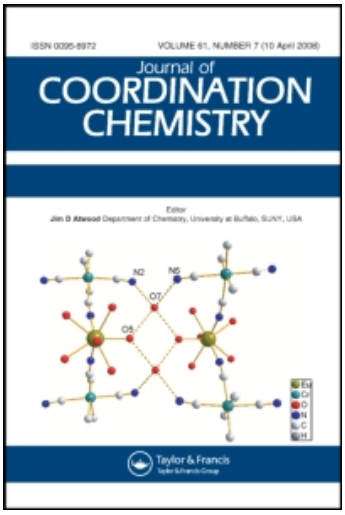

Journal of Coordination Chemistry
Publication details, including instructions for authors and subscription information:
http://www.informaworld.com/smpp/title~content=t713455674

MAGNETIC PROPERTIES AND ELECTRONIC STRUCTURE OF FIVE- AND SIX-COORDINATE MANGANESE(II)2,6-*bis*(BENZIMIDAZOL-2-YL) PYRIDINE COMPLEXES

Wolfgang Linert[a]; Franz Renz[a]; Roman Boca[b]
[a] Institute of Inorganic Chemistry, Technical University of Vienna, Vienna, Austria [b] Department of Inorganic Chemistry, Slovak Technical University, Bratislava, Slovakia

To cite this Article Linert, Wolfgang , Renz, Franz and Boca, Roman(1996) 'MAGNETIC PROPERTIES AND ELECTRONIC STRUCTURE OF FIVE- AND SIX-COORDINATE MANGANESE(II)2,6-*bis*(BENZIMIDAZOL-2-YL) PYRIDINE COMPLEXES', Journal of Coordination Chemistry, 40: 4, 293 — 309
To link to this Article: DOI: 10.1080/00958979608024534
URL: http://dx.doi.org/10.1080/00958979608024534

J. Coord. Chem., 1996, Vol. 40, pp. 293–309
Reprints available directly from the publisher
Photocopying permitted by license only

MAGNETIC PROPERTIES AND ELECTRONIC STRUCTURE OF FIVE- AND SIX-COORDINATE MANGANESE(II)2,6-*bis*(BENZIMIDAZOL-2-YL) PYRIDINE COMPLEXES

WOLFGANG LINERT[a,*], FRANZ RENZ[a] and ROMAN BOCA[b]

[a]*Institute of Inorganic Chemistry, Technical University of Vienna, Getreidemarkt 9/153, A-1060 Vienna, Austria;* [b]*Department of Inorganic Chemistry, Slovak Technical University, SK-812 37 Bratislava, Slovakia*

(Received 30 April 1996)

Two manganese(II) complexes with the terdentate ligand 2,6-*bis*(benzimidazol-2-yl)pyridine, namely $[Mn(bzimpy)_2(ClO_4)_2]$, **1** and $[Mn(bzimpy)Cl_2]\cdot 0.5MeOH$, **2**, have been investigated by magnetic susceptibility measurements in the temperature range 18 to 300 K. Electron spin resonance has been measured in solid state and frozen solution at 77 K. Parameters for the magnetic contributions to the Hamiltonian obtained by these techniques confirm axial magnetic anisotropy. ACS data are: $g_{av} = 1.92 \pm 0.04$, $|D/hc| = 0.9 \pm 1.3$ cm^{-1} and $g_{av} = 1.89$, $|D/hc| = 1.4$ cm^{-1} for **1** and **2**, respectively. The three found ESR resonances correspond to $g_{eff}(1) = 1.99$, $g_{eff}(2) = 3.3$ and $g_{eff}(3) = 4.3$. The highest field resonance exhibits a hyperfine sextet splitting of $|A_{av}/hc| = 92 \times 10^{-4}$ cm^{-1} for both complexes. Well resolved forbidden transitions allow for an estimation of the zero-field splitting parameter being $D/hc = -0.09$ and 0.13 cm^{-1} for the two complexes, respectively. *Ab initio* MO-LCAO-SCF calculations on a double-zeta basis set indicate that complex **2** should be more stable than **1**. The calculations also yielded information on electronic structure, bond-strengths and charge distribution within the complexes.

Keywords: Manganese(II); benzimidazole; magnetochemistry; e.s.r.

Mixed ligand coordination of two bidentate ligands (L_{NN}) such as 2,2′-bipyridine and 1,10-phenanthroline with two monodentate ligands (L′) may generate variable stereochemistry in metal complexes. For example hexacoordinated *cis*-$[M(L_{NN})_2L'_2]$ or pentacoordinated $[M(L_{NN})_2L']$ complexes may be formed. The shape of the coordination polyhedron for the second class may vary between trigonal bipyramidal and tetragonal pyramidal arrangements depending on the nature of the ligand L′. Such complexes might be compared with

* Author for correspondence.

complexes containing two terdentate ligands (L_{NNN}), exemplified by 2,6-*bis*(benzimidazol-2′-yl)pyridine, bzimpy, below.

Its hexacoordinate complexes *mer*-$[M(L_{NNN})_2]^{2+}$ have been well characterized for M = Mn^{2+}, Fe^{2+}, Co^{2+}, Ni^{2+}, Cu^{2+} and Zn^{2+}.[1–3] However, pentacoordinate complexes of $[M(L_{NNN})X_2]$ type also are known for M = Mn^{2+}, Cu^{2+} and Zn^{2+}.[3–5] Some of these complexes, particularly when hexacoordinate Fe(II) centres are involved, exhibit spin crossover behaviour. It is therefore of great interest to clarify conditions leading to the formation of hexacoordinate and/or pentacoordinate complexes of bzimpy (hereafter **L**). For this purpose we prepared $[Mn(bzimpy)_2](ClO_4)_2$ and $[Mn(bzimpy)Cl_2]\cdot 1/2MeOH$ complexes for a detailed study by magnetic susceptibility measurements, electron spin resonance, and quantum chemical calculations with respect to their electronic structure.

EXPERIMENTAL

Ligand and Complexes

The ligand 2,6-*bis*(benzimidazol-2′-yl)pyridine (**L**) was synthesized according to the literature[6] and recrystallized three times from methanol. The metal salts $Mn(ClO_4)_2\cdot 6H_2O$ and $MnCl_2\cdot 2H_2O$ (Fluka, p.a.) were used as received. The complexes were prepared by mixing hot methanolic solutions of bzimpy (*ca* 1 g/cm^3) with stoichiometric amounts of the respective metal salt dissolved in a minimum volume of methanol. The precipitated manganese(II) complexes were filtered off, washed twice with cold methanol and dried *in vacuo* over $CaCl_2$ (yield more than 90%). Analytical data for the obtained yellow salt $[Mn(bzimpy)_2](ClO_4)_2$ are: Found: C, 51.0; H, 2.94; Cl, 7.90; N, 15.5% Calc. for $C_{38}H_{27}Cl_2MnN_{10}O_8$: C, 52.1; H, 2.99; Cl, 8.09; N, 16.0%. For the yellow salt $[Mn(bzimpy)Cl_2]$: Found: C, 51.8; H, 3.68; N, 15.6%. Calc. for $C_{19}H_{13}Cl_2MnN_5\cdot 0.5CH_4O$: C, 51.68, H, 3.34, N, 15.45%.

The existence of volatile components in **2** was confirmed by thermal measurements (Q-derivatograph). The TG curve shows a loss of 3.6 mg of the total 100 mg sample mass with heating to 250°C with a minimum at 151°C at the DTG curve. The composition of $[Mn(bzimpy)Cl_2]\cdot 0.5MeOH$ implies 3.54% of volatile component. The presence of the methanol in the crystal structure has been shown by electron impact mass spectroscopy (peaks appearing at 32, 29 and 28 m/e).

Since the presence of iron impurities may produce an ESR signal, the iron content was analysed by atomic absorption spectroscopy (Zeiss, AAS3 equipment; methanol solution of **2**, acetylene-O_2 flame). No traces of iron were detected.

Magnetic Susceptibility Measurements

The temperature dependence of the powder magnetic susceptibility has been recorded using an AC susceptometer (Lake Shore, models 7221 and 7130). The field parameters were: frequency $f = 666.7\ s^{-1}$ and field intensity $H_{AC} = 320\ A\ m^{-1}$. The temperature range was limited by liquid nitrogen used as cryogenic medium (77 K) and/or a helium refrigerator (18 K). Correction for diamagnetism have been neglected but the signal of the sample holder filled by helium gas has been subtracted.

Electron Spin Resonance

ESR spectra were recorded on an X-band spectrometer (Bruker ER 200D SRC). The sample was inserted into a quartz tube having 0.4 cm outer diameter and 0.05 cm wall thickness. A good amorphous structure was obtained by a rapid cooling of a methanolic solution in liquid nitrogen.

Molecular Orbital Calculations

Electronic structure calculations have been carried out by *ab initio* MO-LCAO-SCF methods.[7] The basis set corresponds to the double-zeta quality: Wachters set (14s9p5d) contracted to [8s5p3d] for manganese[8] and Huzinaga sets for main-row elements, namely, (14s11p) → [6s4p] for chlorine (8s4p) → [4s2p] for carbon and nitrogen, and (4s) → [2s] for hydrogen atoms. Although utilization of the C_{2v} symmetry of the complexes would be possible, C_1 symmetry has been assumed and the calculations have been done within the restricted Hartree-Fock approach for open shell systems. Thus 570 molecular orbitals for **1** and 340 for **2** have been evaluated. The population analysis involves the standard Mulliken procedure as well as the shared-electron-number procedure with two-centre (SEN-2) and polycentre (SEN-n) corrections, respectively.[9]

In order to accomplish geometry optimization, an approximate, but non-empirical version of the *quasi*-relativistic INDO/1 (intermediate neglect of differential overlap) method has been applied.[10–11] The unrestricted Hartree-Fock approach has been used for open shell systems and calculated spin densities have been projected in order to eliminate admixtures of higher multiplicity components. As projected spin densities do not alter significantly, they were omitted from subsequent presentation. Solvent effects have been included using a modified Germer (continuous) model of solvation, where the solvent properties are involved *via* the relative permittivity ($\varepsilon_r = 33$).[12]

RESULTS AND DISCUSSION

Magnetochemical Measurements

The recorded mass susceptibility has been converted to molar susceptibility and the data were processed first by a non-linear regression to fit the extended Curie-Weiss law (**1**). Accordingly the molar Curie constant is where S = 5/2 denotes the spin number for Mn^{2+}. The universal constants N_A = Avogadro number, μ_0 = permeability of vacuum, μ_B = Bohr magneton and k = Boltzmann constant enter the reduced Curie constant $C_0 = N_A\mu_0\mu_B^2/k$. The other symbols in (**1**) are Θ, the Weiss constant, and α_{mol}, the overall temperature-independent term. The quantity α_{mol}^{dia} is the sum of diamagnetic terms, and temperature independent paramagnetism, α_{mol}^{TIP}. Pascal's constants[13] have been used to estimate $\alpha_{mol}^{dia}(\mathbf{1}) = -5.83 \times 10^{-9}$ m^3 mol^{-1} and $\alpha_{mol}^{dia}(\mathbf{2}) = -3.23 \times 10^{-9}$ m^3 mol^{-1}. For the free ligand bzimpy, α_{mol}^{dia} (**L**, Pascal) $= -2.40 \times 10^{-9}$ m^3 mol^{-1}. This value is comparable with the experimental determination[2] based on the Evans method utilizing the NMR shift: α_{mol}^{dia}(**L**, NMR) $= -2.66 \times 10^{-9}$ m^3 mol^{-1}. Direct measurements of the temperature dependence of the magnetic susceptibility for the ligand bzimpy shows that the molar susceptibility keeps the value of χ_{mol} (**L**, ACS) $= +6.5 \times 10^{-9}$ m^3 mol^{-1} thus indicating a contribution to the temperature-independent paramagnetism.

$$\chi_{mol} = C_{mol}/(T - \Theta) + \alpha_{mol} \quad (1)$$

$$C_{mol} = C_0 g_{av}^2 S(S + 1)/3 \quad (2)$$

In calculating the effective magnetic moment, μ_{eff}, two formulae were applied. The usual expression is (**3**) where the molar susceptibility is corrected to diamagnetism.

These values will deviate from linearity at low temperature. The second formula, (**4**), accounts for the Weiss constant.

This function follows the scattering of $C_{mol}^{1/2}$ *vs* T and it is almost constant, even at low temperatures.

$$\mu_{eff}/\mu_B = [(3k/N_A\mu_0)\, T(\chi_{mol} - \alpha_{mol}^{dia})]^{1/2} \quad (3)$$

$$\mu'_{eff}/\mu_B = [(3k/N_A\mu_0)(T - \Theta)(\chi_{mol} - \alpha_{mol}^{dia})]^{1/2} \quad (4)$$

The temperature dependences of χ_{mol}, C_{mol} and μ'_{eff} are shown in Figure 1 and Figure 2. A good test for the validity of Curie-Weiss behaviour is obtained when

the test function $(T - \Theta)(\chi_{mol} - \alpha_{mol})$ *vs* T follows straight line with zero slope (*i.e.*, the Curie constant, C_{mol}). It can be seen that both complexes follow the Curie-Weiss law almost perfectly; the test function C_{mol} *vs* T has zero slope. Important magnetochemical data are collected in Table I.

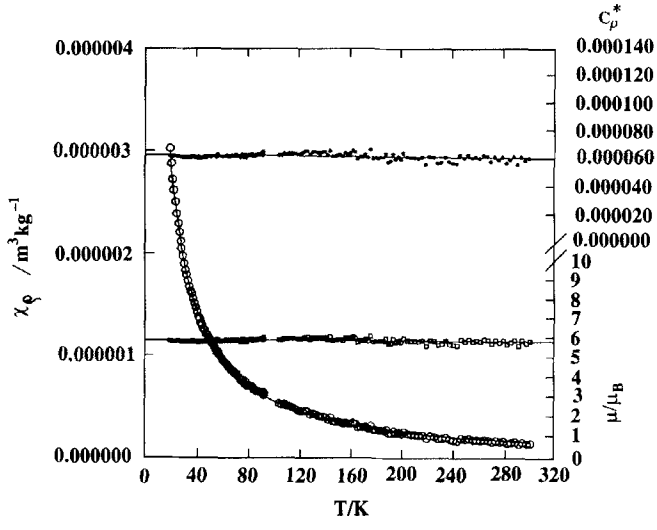

FIGURE 1 Temperature-dependent magnetic data for **1**: Open circles - mass susceptibility χ_ρ (*left*); filled circles - test function C_ρ^*; open squares - magnetic moment μ_{eff}/μ_B.

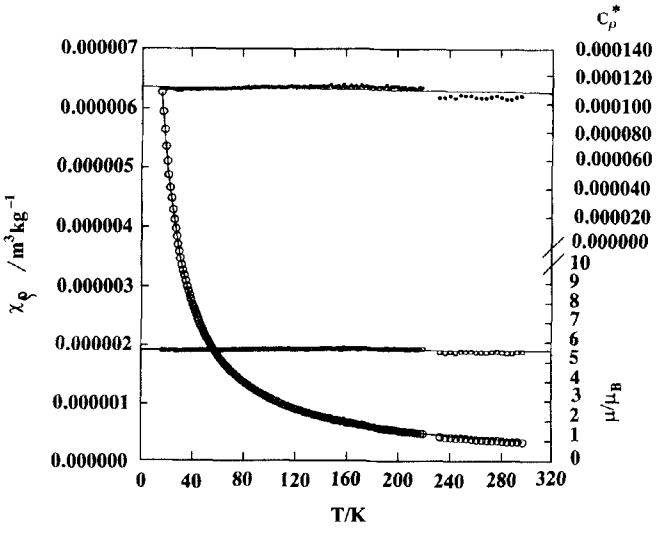

FIGURE 2 Temperature-dependent magnetic data for **2**: Open circles - mass susceptibility χ_ρ (left); filled circles - test function C_ρ^*; open squares - magnetic moment μ_{eff}/μ_B.

TABLE I Magnetic susceptibility data

	Data set					
Quantity	*1a*	*1b*[#]	*1c*	*2d*	*2e*[2]	*2f*
A) C-W fit						
T/K	77–300	77–220	18–220	77–300	77–220	18–220
Points	111	68	127	111	69	143
R-factor/%	0.90	0.94	1.55	0.41	0.45	0.31
g_{av}(CW)	2.058	2.006	1.974	2.007	1.990	1.908
Θ/K	–8.14	–6.44	–0.901	–6.82	–6.14	–0.374
$\alpha_{mol}/10^{-9}m^3mol^{-1}$	–40.6	–30.8	–58.7	–34.0	–32.4	–11.3
μ_{eff}/μ_B	6.09	5.94	5.84	5.94	5.89	5.65
B) ZFS fit, D > 0						
T/K			18–91			18–91
Points			73			75
R factor			0.64			0.20
g_{av}(ZFS)			1.924 ± .04			1.891
D/hc/(cm^{-1})			0.92 ± 1.43			1.47
$\alpha_{mol}/10^{-9}m^3mol^{-1}$			–26.8 ± 4.3			0
C) ZFS fit, D < 0						
R factor/ %			0.64			0.20
g_{av}(ZFS)			1.924 ± 0.04			1.890
D/hc/(cm^{-1})			–0.89 ± 1.32			–1.38
$\alpha_{mol}/10^{-9}m^3mol^{-1}$			–26.8 ± 4.3			0

[#] Data set corrected for sample holder signal.

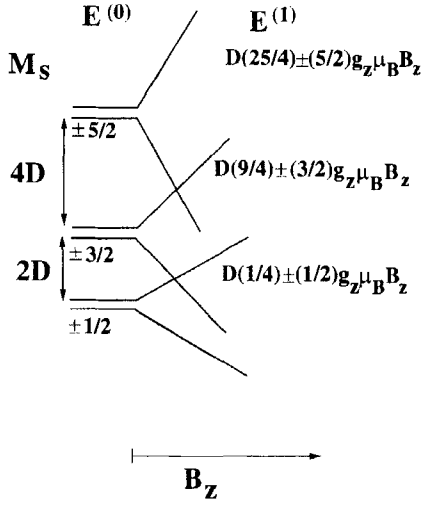

FIGURE 3 Schematic representation of the zero-field splitting for the S = 5/2 spin system.

The value of μ'_{eff} differs only slightly from the spin only value of 5.92 μ_B for five unpaired electrons. The negative value of the Weiss constant, however, indicates an antiferromagnetic interaction in the solid state. The value of Θ includes intermolecular exchange coupling (zJ), zero-field splitting (D) and g-factor asymmetry $(g_\perp^2 - g_{||}^2)/(2g_\perp^2 + g_{||}^2)$. Correction for the sample holder signal slightly alters the values of the Curie-Weiss parameters and was preferably used for the temperature interval 77 to 220 K for reasons explained elsewhere.[14]

Data sets recorded above 18 K produce quite smaller values of Θ and were used to calculate zero-field splitting (ZFS) parameters. The ZFS, owing to the spin-orbit interaction, separates the spin states with spin projections $M_s = \pm 1/2, \pm 3/2$ and $\pm 5/2$ by 2D and 4D, respectively (Figure 3).

The molar magnetic susceptibility of a powder sample for an axial system with the spin quantum number S = 5/2 is described by to (9).[15]

$$\chi_{mol} = (2\chi_\perp + \chi_{||})/3 + \alpha_{mol} \tag{5}$$

$$\chi_{||} = (C_{||}/4T)(1 + 9e^{-2x} + 25e^{-6x})/(1 + e^{-2x} + e^{-6x}) \tag{6}$$

$$\chi_\perp = (C_\perp/4T)[9 + (8/x)(1 - e^{-2x}) + (5/2x)(e^{-2x} - e^{-6x})]/(1 + e^{-2x} + e^{-6x}) \tag{7}$$

$$x = D/kT \tag{8}$$

$$C_\perp \cong C_{||} = C_0 g_{av}^2 \tag{9}$$

Fitting χ_{mol} *vs* T requires at least three adjustable parameters, D, α_{mol} and g_{av}. Since the powder data can hardly be used to determine the sign of the D parameter, the fitting procedure has been done twice under the constraint of either $D > 0$ or $D < 0$. Both sets of magnetic parameters are identical for **1** and $|D/hc| = 0.9 \pm 1.4$ cm^{-1}. The value of g_{av} is the same (within experimental error) when calculated from the Curie-Weiss law (1.97) or the zero-field splitting equations (1.92). The assumption of an axial (D_{4h}) symmetry is no longer valid for **2** exhibiting a symmetry lower than C_{2v}. Thus a more complex analysis, also involving the rhombic ZFS parameter E, is necessary for the three components of the magnetic susceptibility. The data presented in Table I (g_{av} = 1.89, $|D/hc| = 1.4$ cm^{-1}) serve only as the first estimates (for this reason error estimates are omitted).

Electron Spin Resonance

The solid state ESR spectrum of **1** at 77 K exhibits a central hyperfine sextet, whereas the ESR spectrum of **2** is characterized by bands with effective g values of $g_{eff}(1) = 2.0$, $g_{eff}(2) = 3.3$ and $g_{eff}(3) = 4.3$. The ESR spectrum of a frozen methanol solution of **1** (Figure 4) exhibits all three main bands with $g_{eff} = 2.0$, 3.3 and 4.3 (the presence of iron(III) is excluded on the basis of analytical data).

It is obvious that in a well resolved central hyperfine sextet ($g_{eff} = 2.0$) some additional lines are present. It is possible that ESR spectra, involving interactions with nuclei with quadrupole moments (nuclear spin $I > 1$), vizualize a violation of the selection rules. This is the case in that in addition to the transitions due to $\Delta M_S = \pm 1$, $\Delta M_I = 0$, transitions associated with $\Delta M_I = \pm 1$ occur. This effect is seen as weak lines midway between the principal hyperfine lines. The forbidden lines are themselves split into doublets by spin-spin interaction of the sextuplet state. This causes a variation in the hyperfine splitting separations of the two $\Delta M_I = \pm 1$ transitions which are otherwise degenerate.

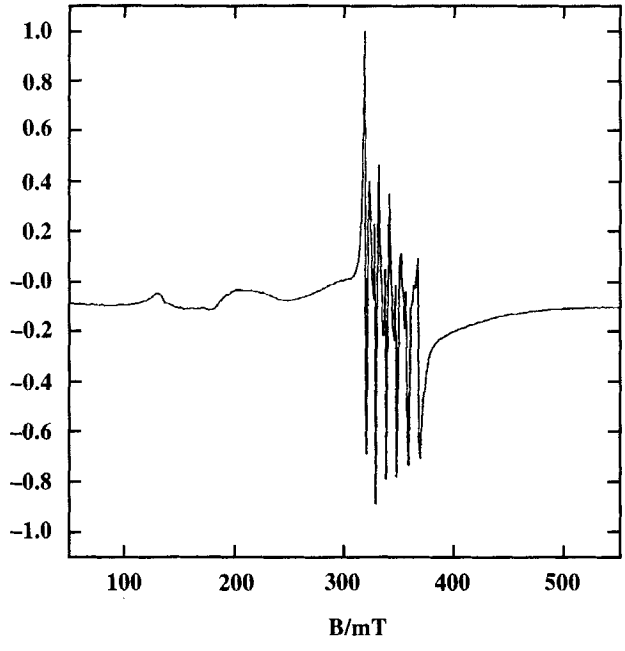

FIGURE 4 ESR spectrum of **1** in frozen (77 K) methanol.

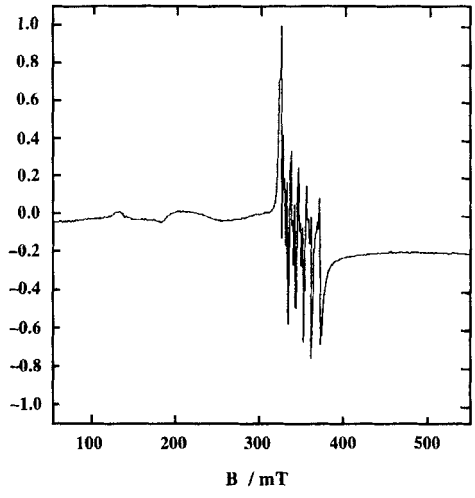

FIGURE 5 ESR spectrum of **2** in frozen (77 K) methanol.

Analogously to **1**, the low temperature (frozen methanol solution) ESR spectrum of **2** gave a well resolved central band with clearly resolved hyperfine as well as forbidden transitions (Figure 5).

The interpretation of ESR spectra principally can be based on two forms of the spin Hamiltonian. In the first form (**10**) the Zeeman term (g-tensor), the hyperfine interaction of the electron-nuclear spin (A^{Mn}-tensor) and the zero-field splitting (axial D and rhombic parameters) are involved. The variables of (10) adopt their usual meaning; the nuclear spin of manganese I^{Mn} equals 5/2. The second, more complex form of the spin Hamiltonian includes some fourth-order terms.

$$\hat{H} = \mu_B \sum_{i=1}^{3} B_i g_i \hat{S}_i + \sum_{i=1}^{3} I_i A_i \hat{S}_i + D[\hat{S}_z^2 - (1/3)\hat{S}^2] + E[\hat{S}_x^2 - \hat{S}_y^2] \quad (10)$$

Both resonances, mid-field with $g_{eff}(1) = 1.99$ and low-field with $g_{eff}(3) = 4.3$ can be interpreted on the basis of the spin Hamiltonian (10) as a consequence of transitions between energy levels of the lowest ($M_S = \pm 1/2$) and the middle ($M_S = \pm 3/2$) Kramers doublets, respectively. A more detailed analysis can be inferred from calculations of the isofrequency curves for the spin Hamiltonian

involving some fourth-order terms where the fine splitting (cubic) parameter a occurs.[16]

Magnetically active centres contributing to the isotropic $g_{eff}(1) = 1.99$ band can be characterized by low values of the fine splitting parameters ($a < 0.05$ cm^{-1}, the values of D and E are also small). Under the condition $2a \approx -3D$, $a > 0.5$ cm^{-1}, $E \approx 0$, the $g_{eff}(3) = 4.3$ resonance is due to the transitions within the energy levels of the lowest Kramers doublet. The centres contributing to this resonance possess the relatively high symmetry of the D_{4h} point group. Because this resonance is almost independent of the E parameter, we cannot exclude the possibility that the symmetry can be even lower. As is seen from the spectra for **1** and **2**, the intensities of these transitions are much lower in comparison with the mid-field resonance $g_{eff}(1) = 1.99$. However, observation of a low-field resonance with $g_{eff}(3) = 4.3$ is not surprising because, from temperature-dependent studies, it is known that at liquid nitrogen temperatures (and higher) the intensity of this low-field resonance is usually small. Several experiments on various systems showed that intensities of both resonances, $g_{eff} \approx 2.0$ and $g_{eff} \approx 4.3$ are rather temperature-independent down to 4 K; the intensity of both resonances tend to increase below 20 K. A resonance with $g_{eff}(2) = 3.3$ seen between the low-field and mid-field resonances is a rare case. The paramagnetic centres contributing to it can be characterized by the symmetry of the D_{4h} point group or lower. This resonance is a consequence of transitions between energy levels of the lowest Kramers doublet.

Forbidden Transitions and Zero-field Splitting

According to the literature[17–18] an estimate of the zero field splitting parameter D in the ESR spectra of randomly oriented paramagnetic species can be obtained from the splitting constants of the allowed hyperfine lines (ΔM_I) corresponding to the central sextet band. Recently, Misra[19] reported a quadratic equation for the D parameter yielding a couple of solutions $D^{(+)}$ and $D^{(-)}$; the values of B_0 (the magnetic field value corresponding to the centre of the hyperfine sextet), ΔB (the splitting of the allowed line of the central sextet into a doublet), A (hyperfine splitting constant) and M_I values enter the cited equation (Figures 6 and 7).

Values of ΔB and the estimated zero-field splitting parameters $D^{(+)}$ and $D^{(-1)}$ ($M_I = 3/2$ used) for the Mn^{2+} ESR spectra for the both complexes thus evaluated are listed in Table II. Note that not all M_I values yield the real roots for D. For this reason the D parameters evaluated in this way serve only as rough estimates.

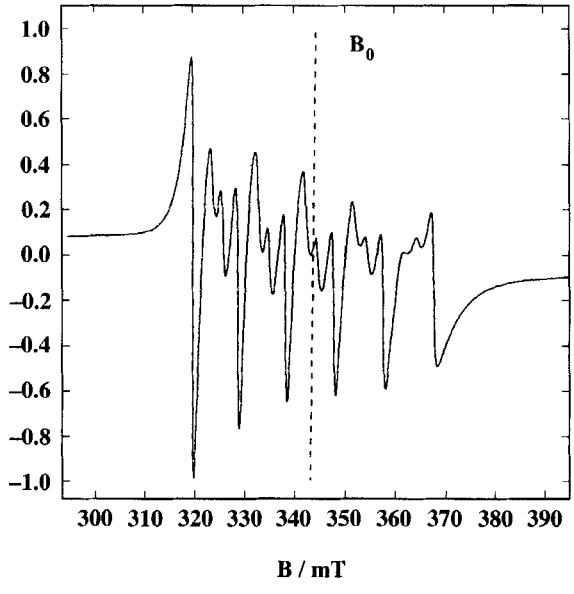

FIGURE 6 Central part of the ESR spectrum of **1** (frozen methanol solution).

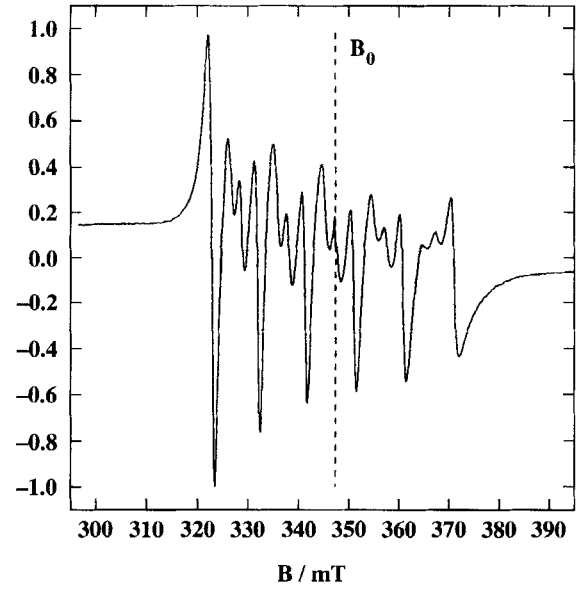

FIGURE 7 Central part of the ESR spectrum of **2** (frozen methanol solution).

TABLE II ESR parameters

	Complex	
Magnetic parameter	*1*	*2*
$g_{eff}(1)$	1.994 ± 0.005	1.991 ± 0.005
$g_{eff}(2)$	3.3 ± 0.1	3.3 ± 0.1
$g_{eff}(3)$	4.3 ± 0.1	4.3 ± 0.1
B_0/mT	342.51	347.28
ΔB_{av}/mT	2.568	2.584
$A_{av}/hc/(10^{-4}\ cm^{-1})$	92.0 ± 1.0	91.9 ± 1.0
$D^{(+)}/hc/(cm^{-1})$	0.133	0.128
$D^{(-)}/hc/(cm^{-1})$	–0.0913	–0.0873

Electronic Structure Calculations

The X-ray structure of $[Mn(bzimpy)_2]^{2+}$ has not been reported. There exists a structural determination of the analogous Fe(II) complex, $[Fe(bzimpy)_2](CF_3SO_3)_2.2EtOH$ (hereafter **3**)[20] which, according to other investigations, is a spin crossover system.[1-2] Thus a structural variation is expected on cooling. For this reason a geometry optimization has been carried out for **1**; its initial geometry has been taken from the X-ray data for **3**. Geometry was optimized with respect to three degrees of freedom: distances R(Mn—N_{py}), R(C_{py}—C_{bzim}) and the angle N_{py}—C_{py}—C_{bzim} (see Figure 8).

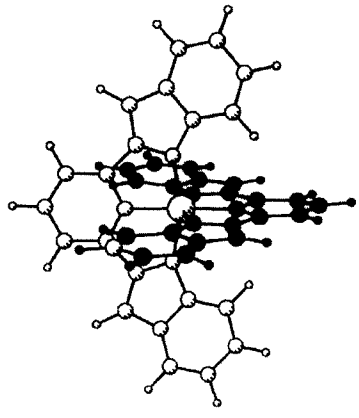

FIGURE 8 Structure of the complex **1**, $[Mn(bzimpy)_2]^{2+}$. Open and filled circles distinguish the two ligands. Atomic coordinates are taken from analogous iron complex.

Independent geometry optimization has been carried out for the low-spin (S = 1/2) and the high-spin (S = 5/2) complexes. The calculated geometry parameters, resulting from the limited geometry optimization, are presented in Table III.

It may be concluded that the high-spin state (S = 5/2) of the complex **1** is more stable (by *ca* 4.7 eV) than the low-spin (S = 1/2) alternative. This finding agrees with magnetochemical data according to which the high-spin state of **1** is stable to 18 K.

Complex **2** differs from [Mn(bzimpy)Cl_2].DMF (hereafter **4**), for which an X-ray structure determination was carried out, in containing crystal solvent.[5] Since pentacoordination can accomodate the crystal solvent as well, geometry variation is possible. Therefore the initial geometry of complex **2** has been taken from X-ray data for **4** and then optimized with respect to five degrees of freedom: the distance R(Mn—Cl) and the angle N_{py}—Mn—Cl are two additional parameters being optimized (see Figure 9).

The optimized geometry shows different axial and equatorial metal-ligand distances: R(Mn—N_a) = 226.3 and R(Mn—N_e) = 220.3 pm (Table IV). These differences are reflected also in the Wiberg (bond-strength) indices; the equatorial bond to the benzimidazole fragment is stronger than the axial bond to the pyridine fragment: W(Mn—N_e) > W(Mn—N_a). The same conclusion is drawn from the bicentric part of the total energy as E(Mn—N_e) < E(Mn—N_a). Thus we conclude that the axial donor atom, N_a (N_{py}), exhibits different donating ability than the equatorial, N_e (N_{bzim}), one.

TABLE III Calculated geometry and energy parameters by QR-INDO/1 method

	Complex				
Geometry	*1 (S=1/2)* C_{2v}	*1 (S=5/2)* C_{2v}	*3 (exptl;Fe)* C_1	*2 (S=5/2)* C_{2v}	*4 (exptl)* C_1
R(Mn—N_{py})/pm	215.9	226.3	192.0	226.5	227.5
			190.4		
R(C_{py}—C_{bzim})/pm	150.7	150.3		150.4	146.7
					145.1
Θ(N_{py}—C_{py}—C_{bzim})/deg	110.3	110.8		110.1	112.0
					112.1
R(Mn—Cl)/pm				237.9	238.5
					234.0
Θ(N_{py}—Mn—Cl)/deg				118.9	105.9
					141.2
R(Mn—N_{bzim})/pm		220.3	193.2		
			199.7		
			193.8		
			199.6		
Total energy/eV	−11167.65	−11172.31		−6613.88	−6603.49

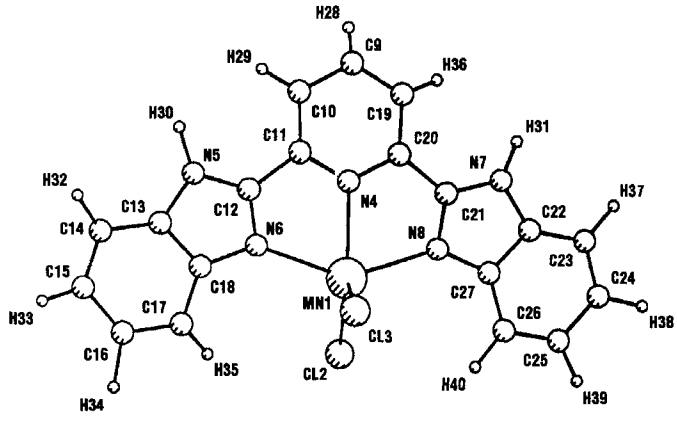

FIGURE 9 Structure of the complex **2**, [Mn(bzimpy)Cl_2].

Spin densities of **1** show partial delocalization over six donor nitrogen atoms: $\rho(N_a)$ = 0.026 (2 x) and $\rho(N_e)$ = 0.024 (4 x) e. Since these values are only 0.5 percent of the central atom spin density [ρ](Mn) = 4.811 e, the super-hyperfine interaction (the A^N-tensor) is not necessarily seen in the ESR spectra.

TABLE IV Calculated bonding characteristics by QR-INDO/1 method

	Complex	
	1	*2*
Distance /pm		
R(Mn—N_a)	226.3	226.5
R(Mn—N_e)	220.3	217.3
Wiberg index		
W(Mn—N_a)	0.373	0.349
W(Mn—N_e)	0.485	0.456
Bicentric energy/eV		
E(Mn—N_a)	−13.46	−13.02
E(Mn—N_e)	−15.87	−15.48
Spin density /e		
$\rho(M_n)$	4.811	4.899
$\rho(N_a)$	0.026	0.015
$\rho(N_e)$	0.024	0.015
In vacuo, ε_r = *1*		
ε_{LUMO}/eV	+0.24	+5.29
ε_{HOMO}/eV	−11.86	−6.32
ε_{SOMO}/eV	−22.5	−15.8
A_1/eV	−0.74	4.42
I_1/eV	11.11	5.68
In solvent, ε_r = *33*		
ε_{LUMO}/eV	+2.40	+5.50

TABLE IV *(Continued)*

	Complex	
	1	*2*
ε_{HOMO}/eV	–9.83	–6.46
ε_{SOMO}/eV	–20.5	–16.1
A_1/eV	2.32	3.47
I_1/eV	5.82	4.50

Results for complex **2** show that the bzimpy ligand is bonded slightly weaker than in **1** as follows from R(Mn—N), W(Mn—N) and E(Mn—N) values. The spin densities on the donor nitrogen atoms drop to $\rho(N) = 0.015$ e and thus there is no reason to consider the A^N-tensor in the analysis of ESR spectra.

The most marked difference between **1** and **2** lies in their frontier molecular orbital energies. A complication arises due to the fact that the Koopmans theorem is violated in metal complexes; the SOMO with a predominant metal d-character often has a lower orbital energy than the HOMO embracing ligand orbitals, but the electron from SOMO is ionized first. Therefore the first electron affinity, $A_1 = E(q-1) - E(q)$, and ionization potential, $I_1 = E(q+1) - E(q)$, were evaluate in an ΔSCF manner (differences in total molecular energies). According to Table IV there is a real effect of solvation on A_1 and I_1 values for **1** (charged system) whereas such an effect is less pronounced for **2** (neutral molecule). Reduction of **1** will be an easy process (A_1 = 2.3 eV) unlike oxidation (I_1 = 5.8 eV), which is energetically unfavourable. This has been observed by cyclic voltammetry for $[Mn(bzimpy)_2](NO_3)_3.3H_2O$ in DMF; reduction at $E_{1/2}$ = –0.44 V was observed and no oxidation until +1.8 V.[5] In **2**, reduction seems as facile as oxidation (A_1 = 3.5 and I_1 = 4.5 eV). In fact, only irreversible reduction of $[Mn(bzimpy)Cl_2]$ in DMF was observed (E_{pc} = 0.03 V).

Using the total molecular energies, as they result from *ab initio* calculations for 'experimental' geometries, complex formation energies were estimated as $E_f(\mathbf{2}) = E(\mathbf{2}) - E(Mn^{2+}) - 2E(Cl^-) - E(L) = -21.3$ eV and $E_f(\mathbf{1}) = E(\mathbf{1}) - E(Mn^{2+}) - 2E(L) = -11.8$ eV.

Although full geometry optimization and correlation effects are not included in these data, they unambiguously show that **2** has a (two-times) higher formation (stabilization) energy relative to **1**.

The charge distributions (Table V) display a considerable dependence on the type of population analysis (SEN-n values appear to be the most realistic). The equatorial N_{bzim} atoms bear more negative charge than the axial N_{py} ones in both complexes. The electron withdrawal effect of the chloro ligands in **2** is reflected in an increased positive charge at the central atom and consequently the negative charges on the nitrogen donor set decrease.

TABLE V *Ab initio* charge distributions for 'experimental' geometries

	Complex 1			*Complex 2*		
Charge/e	*Mulliken*	*SEN-2*	*SEN-n*	*Mulliken*	*SEN-2*	*SEN-n*
Q(Mn)	+1.817	+1.774	+1.804	+1.558	+1.851	+1.839
$Q(N_a)$	–0.959	–0.542	–0.505	–0.773	–0.438	–0.405
	–0.918	–0.485	–0.455			
$Q(N_e)$	–0.834	–0.522	–0.516	–0.751	–0.493	–0.476
	–0.879	–0.553	–0.533	–0.748	–0.485	–0.467
	–0.886	–0.542	–0.524			
	–0.862	–0.529	–0.505			
Q(Cl)				–0.792	–0.930	–0.946
				–0.837	–0.933	–0.951
d^5(Mn)	5.13			5.12		

Magnetic susceptibility measurements in the temperature range 18 to 300 K show that both complexes retain their high-spin state, S = 5/2; the effective magnetic moment does not deviate significantly from the spin-only value. The complexes exhibit only slight (or moderate) zero-field splitting of the order of D/hc = ±1 cm^{-1}. The energy levels E_i = 0, 2D and 6D have almost the same Boltzmann occupation at temperatures as low as 18 K (N_i = 0.40, 0.34 and 0.26 for M_s = ±1/2, ±3/2 and ±5/2 at 18 K and |D/hc| = 0.9 cm^{-1}). For this reason Curie-Weiss behaviour is followed almost perfectly in the higher temperature range. Increased magnetic anisotropy with higher |D/hc| = 1.4 cm^{-1} is indicated for the pentacoordinate complex **2**. The averaged g-values, g_{av} = 1.92 for **1** and g_{av} = 1.89 for **2**, account for the magnetic activity (population) of all three Kramers doublets. On the contrary, the effective g-values, g_{eff} = 1.99, 3.3 and 4.3, deduced from ESR resonances account only for allowed intra-doublet (M_s = ±1/2) or inter-doublet (M_s = –1/2 to –3/2, +1/2 to +3/2) transitions at X-band frequency (*ca* 9.4 GHz) and applied field up to 0.8 T. Thus there is no basis for an exact match of ACS and ESR parameters. The ESR data indicate axial (D_{4h}) magnetic symmetry, but this may be lower. In addition, well resolved forbidden transitions allow estimation of the order of the D values. *Ab initio* calculations explain the relative stability of **2** *vs* **1**. INDO/1 calculations confirm that the axial Mn—N_{py} bond is weaker than the equatorial Mn—N_{bzim} one.

$$N_i = e^{-Ei/kT}/(1 + e^{-2D/kT} + e^{-6D/kT}) \qquad (11)$$

Acknowledgments

Thanks are due to the fonds 'Zur Forderung der wissenschaftlichen Forschung in Östereich' (Project 10818), the Slovak Grant Agency and to the exchange program between Austria and Slovakia (Project 6 Ös3) for financial support.

Thanks are further due to Marián Valko, Robert Klement and Milan Mazúr from the Department of Physical Chemistry, Slovak Technical University, for assistance concerning ESR measurements.

References

[1] B. Strauss, V. Gutmann and W. Linert, *Monatsh. Chem.*, **124**, 391 (1993).
[2] W. Linert, M. Konecny and F. Renz, *J. Chem. Soc., Dalton Trans.*, 1523 (1994).
[3] S.B. Sanni, H.J. Behm, P.T. Beurskens, G.A. van Albada, J. Reedijk, A.T.H. Lenstra, A.W. Addison and M. Palaniandavan, *J. Chem. Soc., Dalton Trans.*, 1429 (1988).
[4] G. Bernardinelli, G. Hopfgartner and A.F. Williams, *Acta Cryst.*, **C46**, 1642 (1990).
[5] S. Wang, Y. Zhu, F. Zhang, Q. Wang and L. Wang, *Polyhedron*, **11** 1909 (1992).
[6] A.W. Addison and P.J. Burke, *J. Heterocycl. Chem.*, **18**, 803 (1981).
[7] R. Alhrichs, M. Bär, M. Ehring, M. Haser, H. Horn and C. Kolmel, *Program TURBOMOLE* (University of Karlsruhe, 1991).
[8] A.J.H. Wachters, *J. Chem. Phys.*, **52**, 1034 (1970).
[9] C. Ehrhardt and R. Ahlrichs, *Theoret. Chim. Acta*, **68**, 231 (1985).
[10] R. Boca, *Int. J. Quantum Chem.*, **34**, 385 (1988).
[11] R. Boca, *Program MOSEM7*, (Slovak Technical University, Bratislava, 1993).
[12] R. Boca, *Int. J. Quantum Chem.*, **33**, 159 (1988).
[13] E. König, in *Landolt-Börnstein, Neue Serie, Bd. II/2*, (Springer, Berlin, 1996), p. 1.
[14] R. Boca, P. Baran and L. Dlháò, *Chem. Papers*, **48**, 177 (1994).
[15] O. Kahn, *Molecular Magnetism*, (VCH Publishers, New York, 1993).
[16] V. Cerny, B. Petrová and M. Frumar, *J. Non-cryst. Solids*, **125**, 17 (1990).
[17] A. Abragam and B. Bleaney, *Electron Paramagnetic Resonance of Transition Ions*, (Oxford University Press, London, 1970).
[18] F. Mabbs and D. Collison, *Electron Paramagnetic Resonance of d-Transition Metal Complexes*, (*Elsevier*, Amsterdam, 1992).
[19] S.K. Misra, *Physica B*, **203**, 193 (1994).
[20] S. Ruttimann, C.M. Moreau, A.F. Williams, G. Bernardinelli and A.W. Addison, *Polyhedron*, **11**, 635 (1992).